

**Supplemental information**

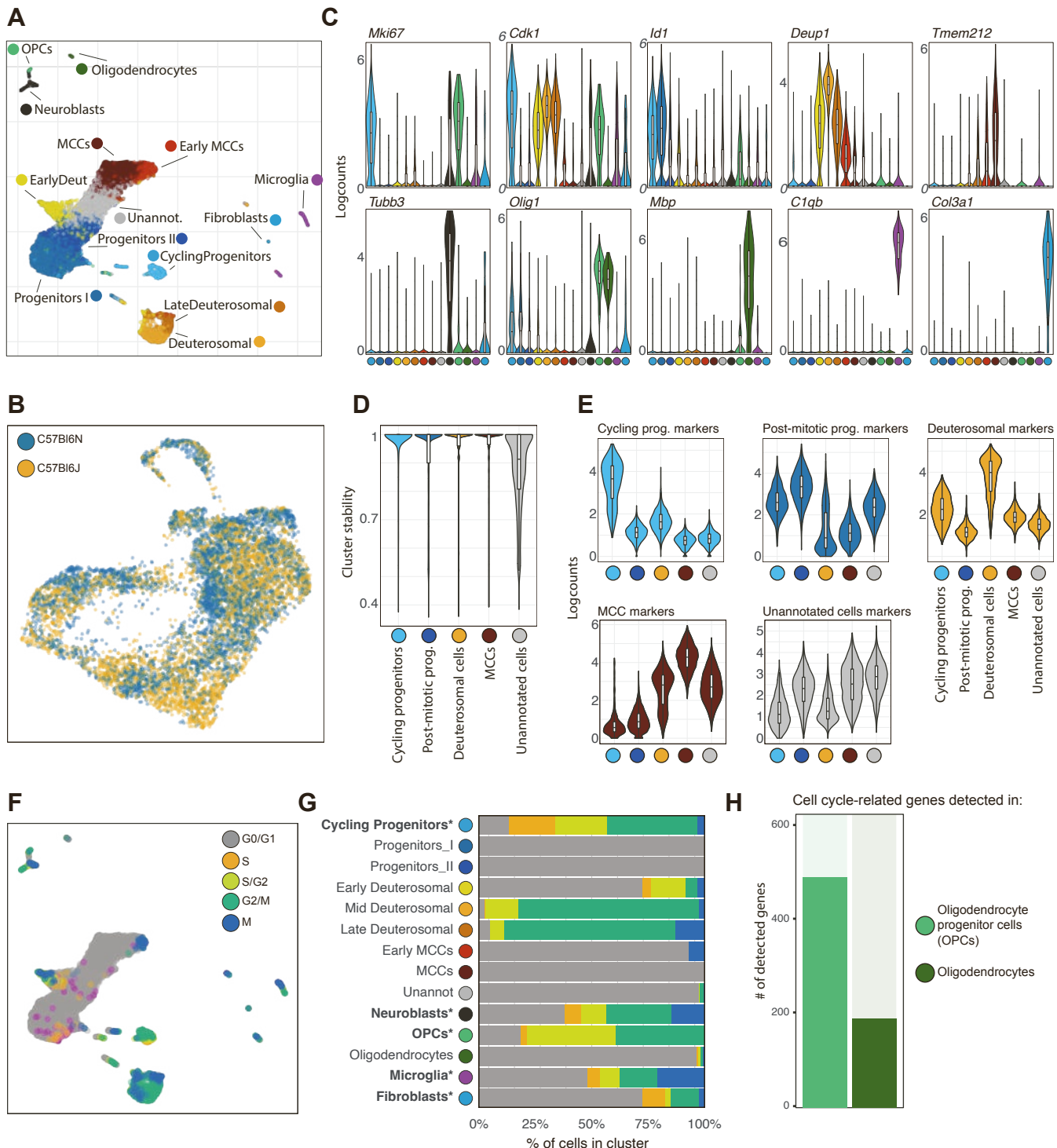
**Cyclin switch tailors a cell cycle variant  
to orchestrate multiciliogenesis**

**Jacques Serizay, Michella Khoury Damaa, Amélie-Rose Boudjema, Rémi Balagué, Marion Faucourt, Nathalie Delgehyr, Laure-Emmanuelle Zaragozi, Pascal Barbry, Nathalie Spassky, Romain Koszul, and Alice Meunier**

## Supplemental figures

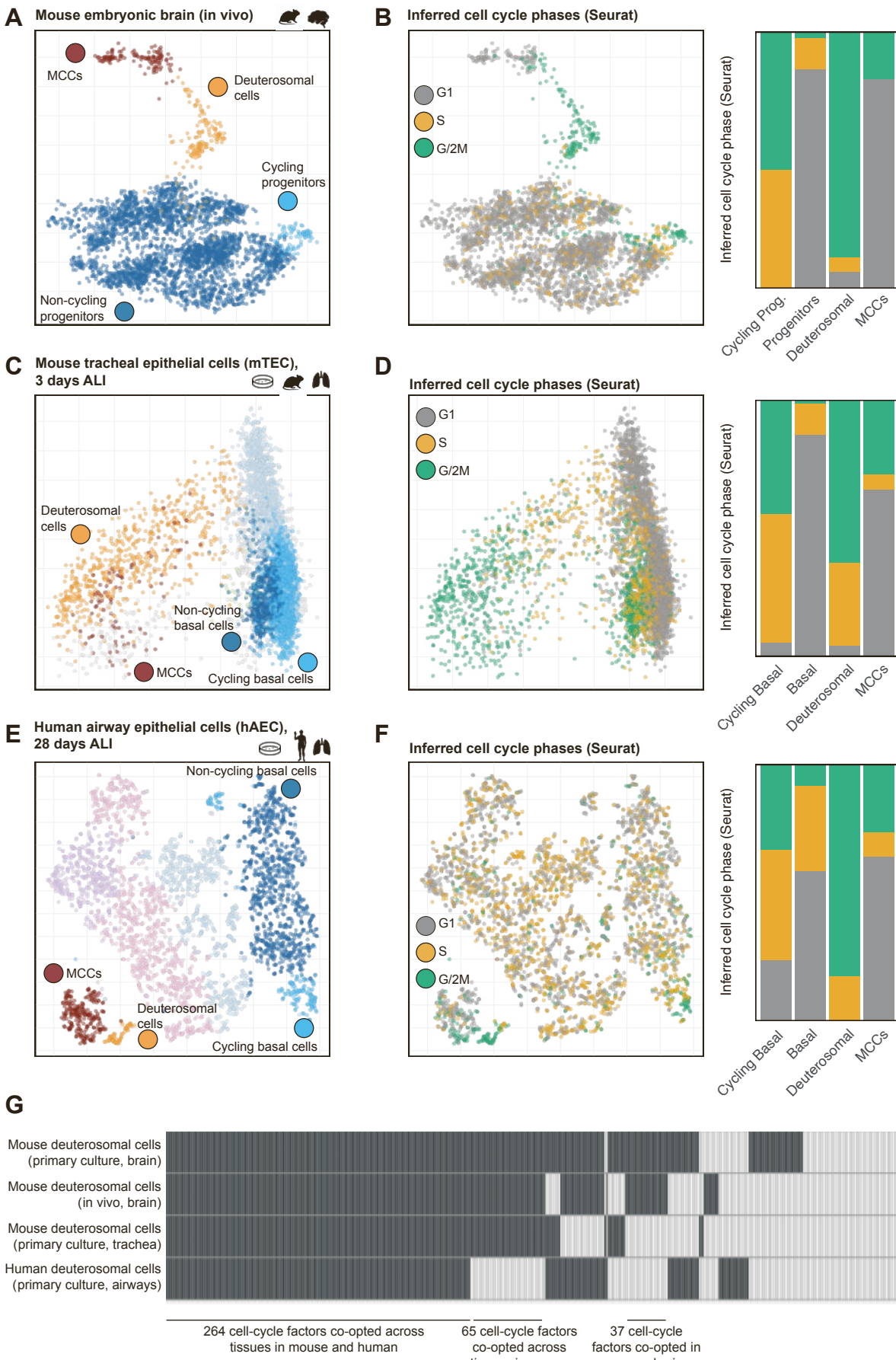
**Figure S1: Single-cell profiling of in vitro differentiating mouse radial glial cells into multiciliated cells, related to Figure 1.**

- (A) Single-cell RNA-sequencing profiling of in vitro differentiating mouse radial glial cells into multiciliated cells. All 16,401 cells are shown in this UMAP projection.
- (B) UMAP projection of cells undergoing MCC differentiation. 4,000 randomly sampled cells from each replicate (C57Bl6N or C57Bl6J) are shown. Colors represent the replicates.
- (C) Expression of known markers of progenitors, differentiating or terminally differentiated MCCs, neuroblasts, OPCs and oligodendrocytes, microglia or stromal cells. Boxplots show the median (horizontal line), the interquartile range (IQR; represented by the height of the box, spanning from the 25th to the 75th percentile), and the whiskers extend from the box to the smallest and largest values within 1.5 times the IQR from the lower and upper quartiles, respectively.
- (D) Stability of cell population clusters. Note that the Unannotated cells have a low cluster stability, indicating that these cells do not reliably form a specific cluster. Boxplots representations are the same as in (C).
- (E) Expression of the top 5 markers of each group of cells, across the five main groups of cells. Boxplots representations are the same as in (C).
- (F) Putative cell cycle phase annotations inferred using SingleR using neural stem cell reference [S1]. All 16,401 cells are shown in this projection.
- (G) Distribution of putative cell cycle phase annotations within each cell population. Cell populations known to proliferate are indicated with an asterisk.
- (H) Number of cell cycle related factors detected in oligodendrocyte progenitor cells (OPCs) and post-mitotic oligodendrocytes (similar to Fig. 1D). A gene is considered expressed in an individual cell population if its expression is greater than 0.5 (logcounts) in at least 20% of the cells within the cell population.



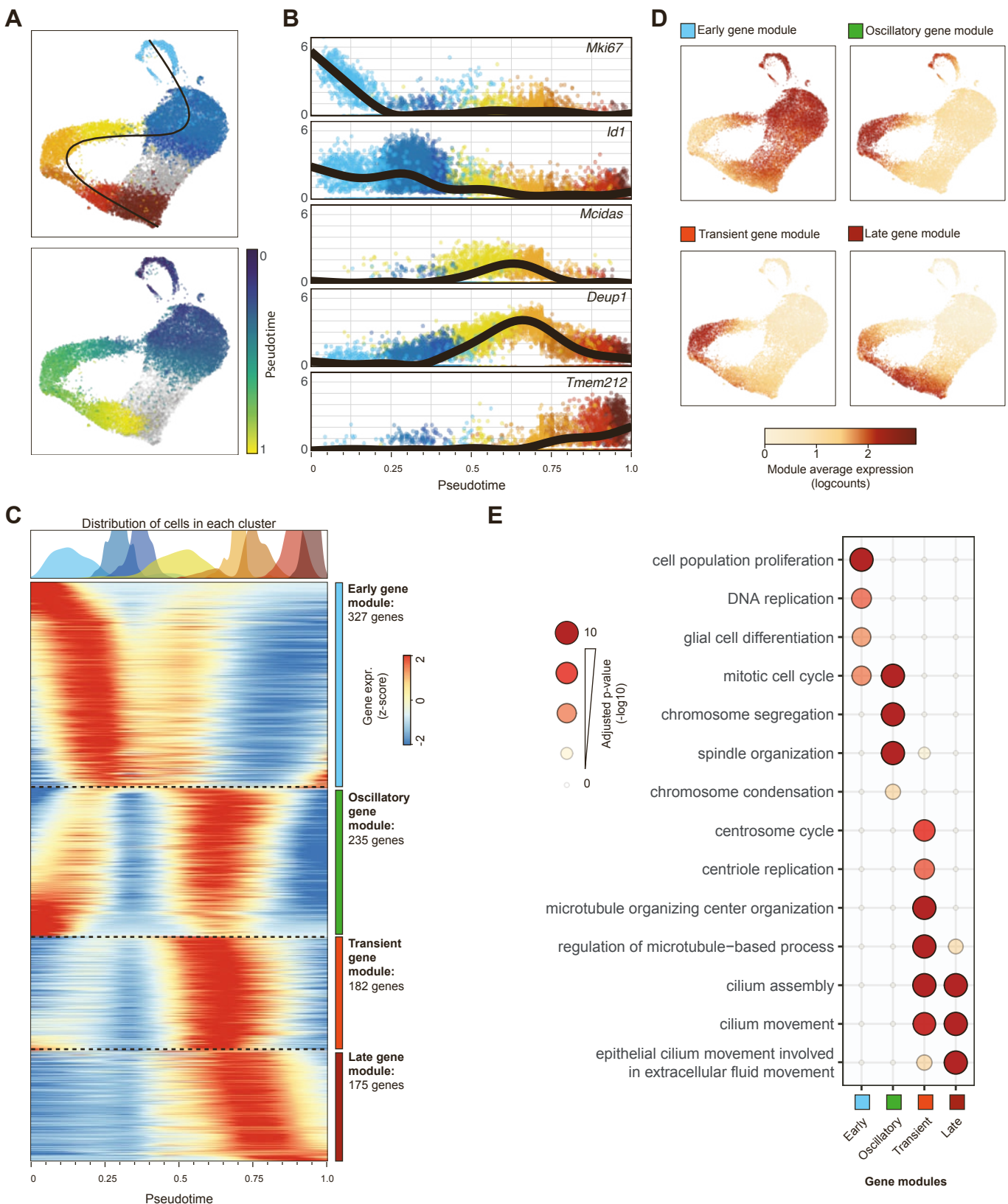
**Figure S2: Cell cycle factors are reused for multiciliation across mammals, related to Figure 1.**

- (A) UMAP embedding of individual transcriptomes from an in vivo scRNAseq experiment performed in brains from mouse embryos [S2]. Color code indicates the different cell groups.
- (B) UMAP embedding of the in vivo brain scRNAseq dataset, with color code indicating the putative cell cycle phase annotations inferred using Seurat (left). Distribution of the putative cell cycle phase annotations in each cell group (right).
- (C) UMAP embedding of individual transcriptomes from an in vitro scRNAseq experiment performed in an air-liquid interface culture of mouse tracheal epithelial cells (mTEC) [S3]. Color code indicates the different cell groups.
- (D) UMAP embedding of the in vitro mTEC scRNAseq dataset, with color code indicating the putative cell cycle phase annotations inferred using Seurat (left). Distribution of the putative cell cycle phase annotations in each cell group (right).
- (E) UMAP embedding of individual transcriptomes from an in vitro scRNAseq experiment performed in an air-liquid interface culture of human airway epithelial cells (hAEC) [S3]. Color code indicates the different cell groups.
- (F) UMAP embedding of the in vitro hAEC scRNAseq dataset, with color code indicating the putative cell cycle phase annotations inferred using Seurat (left). Distribution of the putative cell cycle phase annotations in each cell group (right).
- (G) Summary of cell cycle related factors co-opted in in vitro mouse brain scRNAseq, in vivo mouse brain scRNAseq, in vitro mouse tracheal scRNAseq and in vitro human airway scRNAseq.



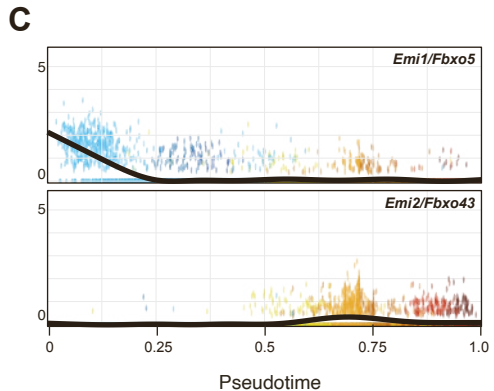
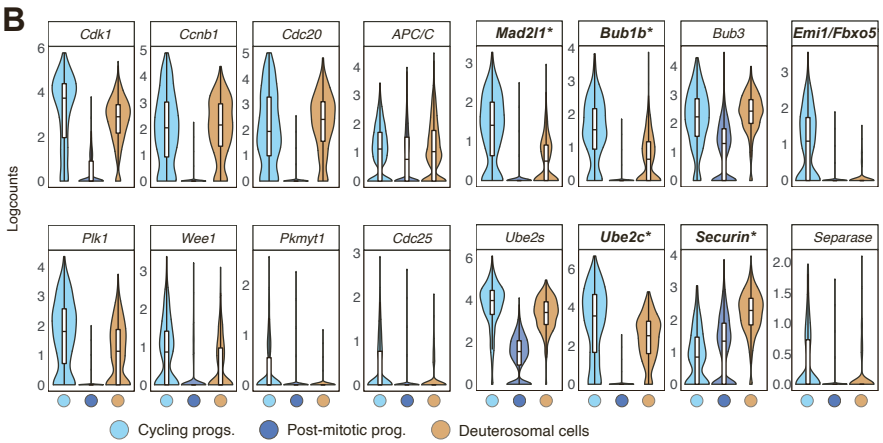
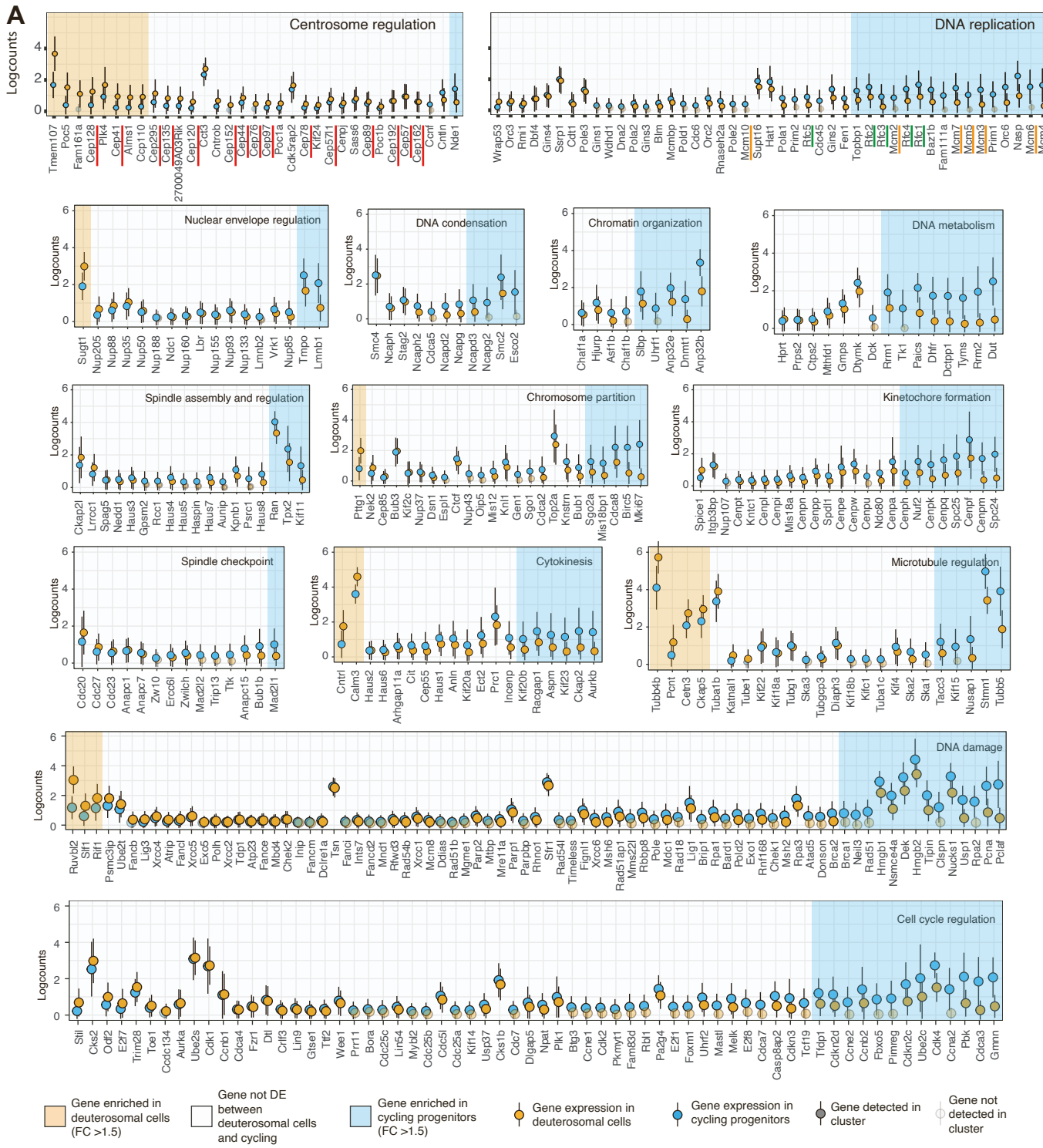
**Figure S3: Lineage of in vitro differentiating mouse radial glial cells, related to Figure 1.**

- (A) Trajectory analysis of in vitro differentiating mouse radial glial cells into multiciliated cells. The cell lineage starts with cycling progenitors, passes through post-mitotic progenitors, deuterosomal cells and finally reaches MCCs. Top: cell lineage embedded in UMAP cell projection. Bottom: UMAP cell projection with cells colored by their inferred pseudotime (rescaled between 0 and 1).
- (B) Temporal expression of *Mki67*, *Id1*, *Mcidas*, *Deup1* and *Tmem212* along the differentiation trajectory shown in (A).
- (C) Aggregated temporal expression of the 919 genes differentially expressed in the scRNAseq dataset. Color scale represents the gene expression (z-scored for each gene independently). On top of the heatmap, the distribution of cells in each cluster is shown. We distinguished four broad patterns of variation of gene expression amongst the 919 genes differentially expressed between cell clusters: a module of “early genes” expressed in progenitors and early deuterosomal cells, a module of “oscillatory genes” (highly expressed in cycling progenitors then silenced in non-cycling progenitors and reactivated in differentiating progenitors), a module of “transient genes” expressed only in deuterosomal cells and a module of “terminal genes” expressed in differentiated MCCs.
- (D) Average expression of each gene module in the UMAP cell projection.
- (E) Gene ontology over-representation analysis for each module depicted in (C). This confirmed that the “oscillatory genes” module was enriched for cell cycle-related processes.



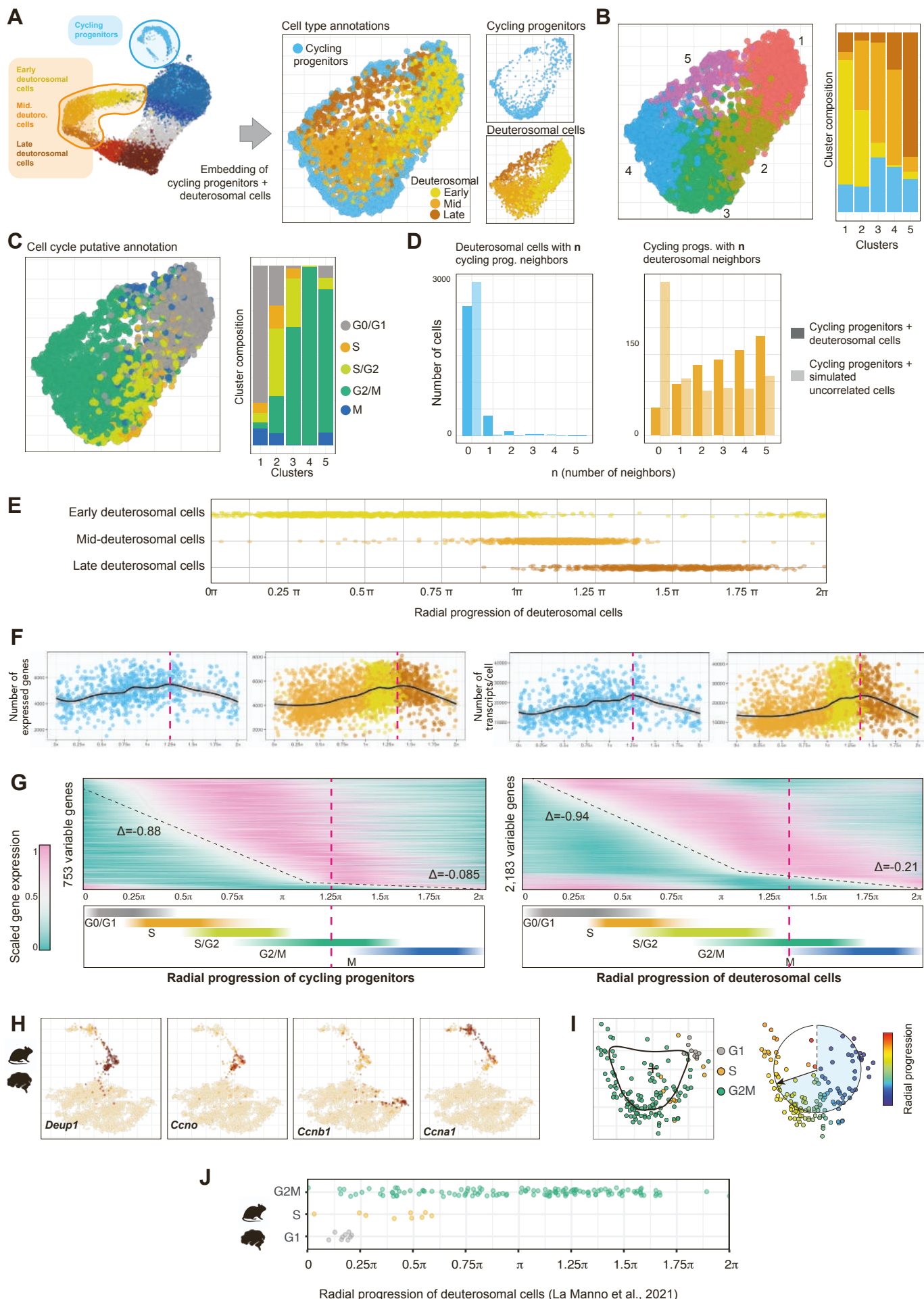
**Figure S4: Factors from all cell cycle subprocesses are re-expressed in deuterosomal cells, related to Figure 2.**

- (A) Expression of cell cycle factors involved in different cell cycle subprocesses, in deuterosomal cells (orange point+ranges) and in cycling progenitors (blue point+ranges). Transparent points denote genes not detected in one or the other cell population. Genes which are not detected in any of the two cell populations are not shown. Gene expression is represented as mean  $\pm$  standard error.
- (B) Violin plot of the expression of the main components of the mitotic oscillator in different cell clusters. Labels in bold indicate factors differentially expressed between deuterosomal cells and G2/M cycling progenitors. Boxplots show the median (horizontal line), the interquartile range (IQR; represented by the height of the box, spanning from the 25th to the 75th percentile), and the whiskers extend from the box to the smallest and largest values within 1.5 times the IQR from the lower and upper quartiles, respectively.
- (C) Temporal expression of *Emi1* and *Emi2* along the differentiation trajectory shown in Fig. S3A.



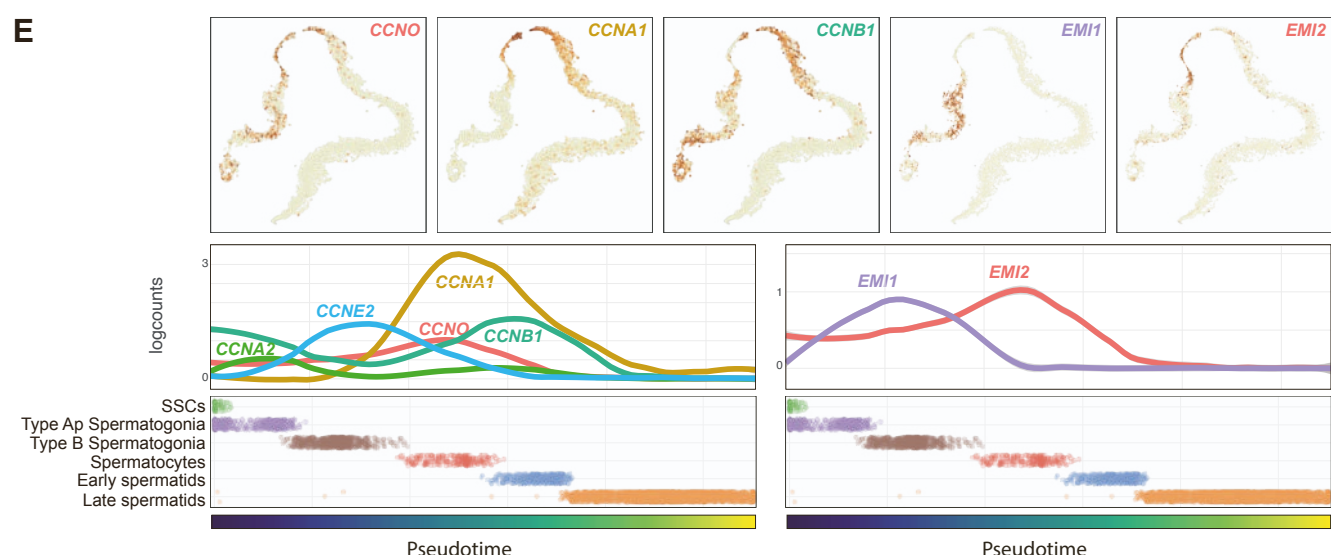
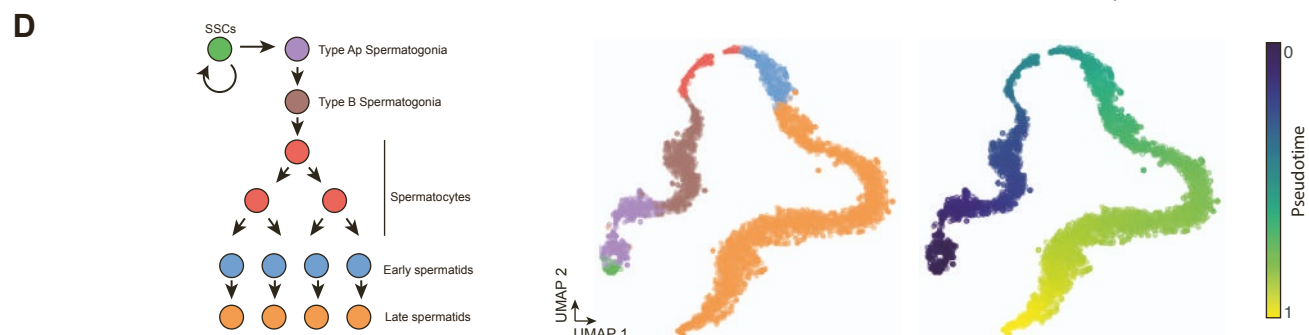
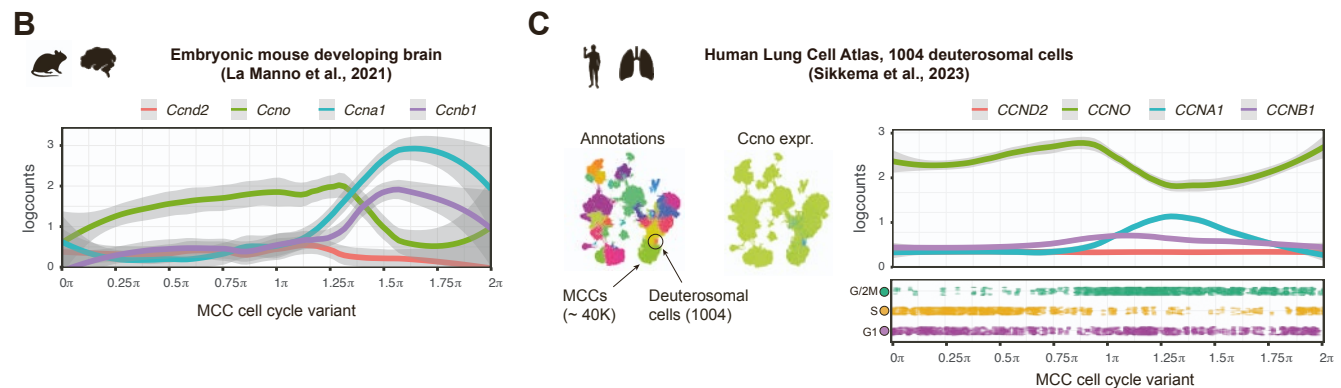
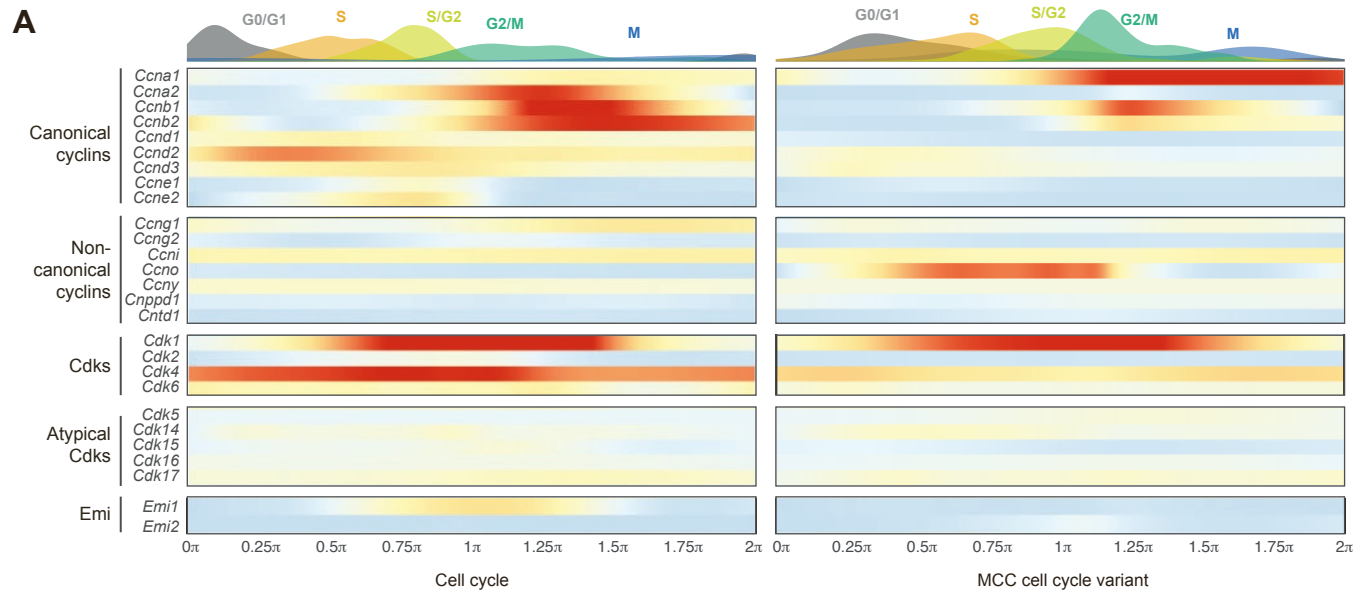
**Figure S5: Sub-processing of cycling progenitors and deuterosomal cells, related to Figure 3.**

- (A) Shared UMAP embedding of all deuterosomal cells and all cycling progenitor cells, showing that cycling progenitors and deuterosomal cells aggregate in close proximity to each other in lower dimensional space.
- (B) Shared cell clustering of all deuterosomal cells and all cycling progenitor cells. Right: proportion of each cell type per cluster. Each of the newly inferred clusters contain a mixture of roughly 15-20% of cycling progenitors and 80-85% of deuterosomal cells.
- (C) Putative cell cycle phase annotations inferred using SingleR using neural stem cell reference [S1]. Deuterosomal cells and cycling progenitor cells are plotted in their shared UMAP embedding. Cycling progenitors and deuterosomal cells in each cluster are enriched for specific cell cycle phases.
- (D) Number of cycling progenitor cells amongst the 5 nearest neighbors for each deuterosomal cell (left) and number of deuterosomal cells amongst the 5 nearest neighbors for each cycling progenitor cell (right). The observed distribution of cycling progenitors / deuterosomal cells amongst the 5 nearest neighbors is shown in solid colors, while the same distribution measured between real cycling progenitors and simulated, uncorrelated cells is shown in transparent.
- (E) Distribution of early, mid- and late deuterosomal cells along their radial progression.
- (F) Number of expressed genes (top) and of transcripts per cells (bottom), in cycling progenitor cells (left) or in deuterosomal cells (right) distributed according to their radial progression.
- (G) Temporal expression of genes which expression vary in cycling progenitor cells (left) or in deuterosomal cells (right). Expression is normalized to the interval [0;1] for each gene, and genes are ordered by the time when 0.5 is crossed from below (seen as a white line). The slope of the white line reports the rate of transcription onsets per unit time. The steeper the slope, the higher the rate is. The rate of transcription onsets is generally constant in cycling progenitor cells and in deuterosomal cells until  $\sim 1.20\pi$ . At this time point, the rate of transcription onsets dramatically decreases (10-fold in cycling progenitors and 4.5-fold in deuterosomal cells).
- (H) Expression of *Deup1* and three cyclins in the in vivo brain scRNAseq dataset [S2].
- (I) Top: PCA embedding (PC1 and PC2) of deuterosomal cells only. The black curve denotes the average position of cells around the center point of the PCA space. Bottom: representation of the deuterosomal cells with a color range indicating the radial progression of each cell.
- (J) Radial distribution of deuterosomal cells with a color scale indicating the putative cell cycle phase annotated using Seurat.



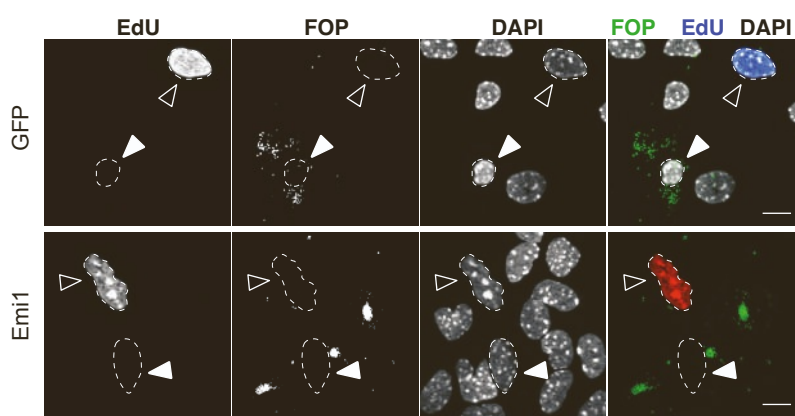
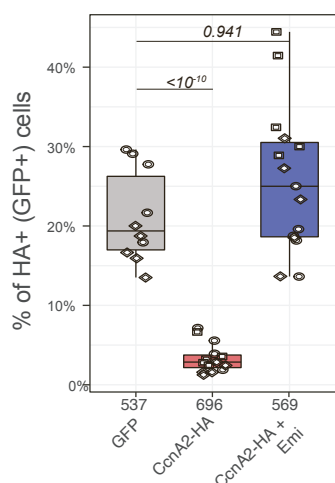
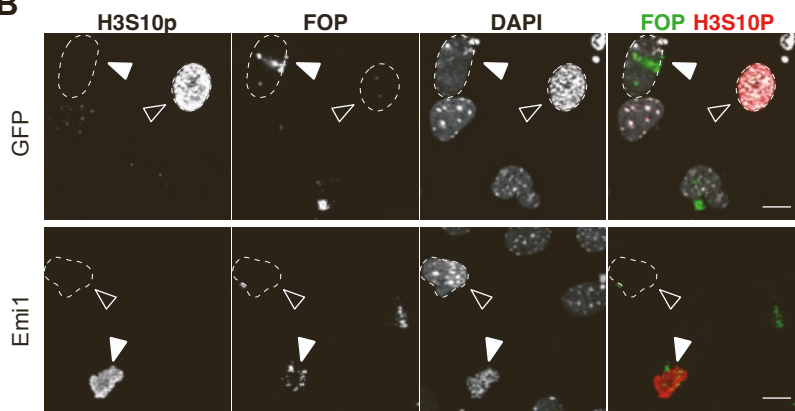
**Figure S6: Expression of cyclins during ciliated cell differentiation, related to Figure 4.**

- (A) Temporal expression of canonical and atypical cyclins along the cell cycle (left) or along the MCC cell cycle variant (right).
- (B) Expression of Cyclin D2 (*Ccnd2*), Cyclin O (*Ccno*), Cyclin A1 (*Ccna1*) and Cyclin B1 (*Ccnb1*) cyclins in deuterosomal cells distributed according to their radial progression, in deuterosomal cells from the embryonic mouse developing brain [S2].
- (C) Expression of Cyclin D2 (*CCND2*), Cyclin O (*CCNO*), Cyclin A1 (*CCNA1*) and Cyclin B1 (*CCNB1*) cyclins in deuterosomal cells distributed according to their radial progression, in deuterosomal cells from the adult human airway epithelium [S4].
- (D) Embedding of a human spermatogenesis scRNAseq dataset [S5] in UMAP 2D dimensional space. Cells are colored by their cell type (middle) or by the pseudotime inferred with slingshot (right). SCCs: Spermatogonial stem cells.
- (E) Expression of Cyclin O (*CCNO*), Cyclin A1 (*CCNA1*) and Cyclin B1 (*CCNB1*) cyclins during spermatogenesis, in UMAP projection (A) or along the inferred pseudotime (B).

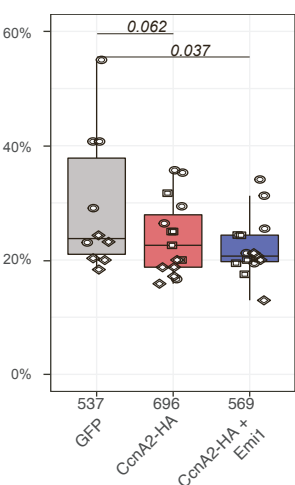
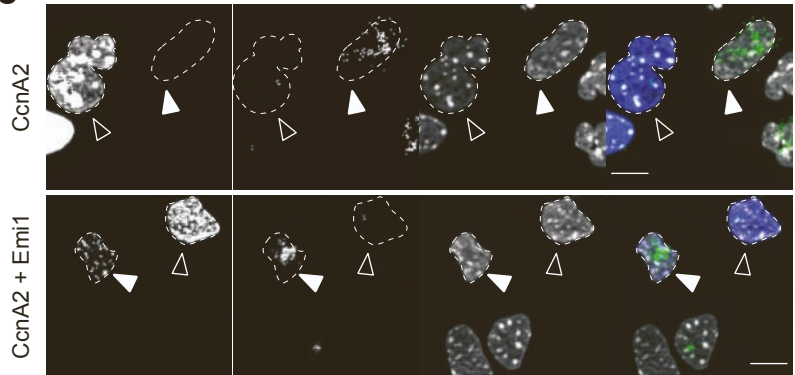
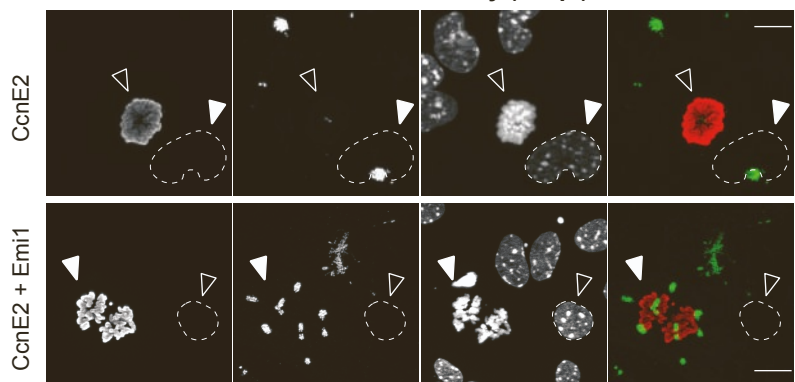


**Figure S7: Canonical Cyclin A2 expression in differentiating MCCs leads to abnormal mitosis figures, related to Figure 5.**

- (A) Representative images of cells infected by *GFP* or *Emi1*, stained for EdU incorporation (24hpi). Centriole staining by FOP is used to identify progenitors (black arrows) and differentiating deuterosomal cells (white arrows). Scale bar = 10 um.
- (B) Representative images of cells infected by *GFP* or *Emi1*, immunostained for mitosis figures (with H3S10p) (96hpi). Centriole staining by FOP is used to identify progenitors (black arrows) and differentiating deuterosomal cells (white arrows). Scale bar = 10 um.
- (C) Representative images of cells infected to express different combinations of cell cycle factors, stained for EdU incorporation (96hpi, top) or for mitosis figures (with H3S10p) (24hpi, bottom). Centriole staining by FOP is used to identify progenitors (black arrows) and differentiating deuterosomal cells (white arrows). Scale bar = 10 um.
- (D) Proportion of HA+ (or GFP) cells (top) and proportion of differentiating cells (bottom) in WT radial glial cell cultures infected by *GFP*, *CcnA2-HA* or *CcnA2-HA+Emi1-Myc*. P-values from batch-corrected t-tests are displayed on top of the graph. The total number of cells counted across the biological replicates is indicated for each experiment: 537 for GFP (2 biological replicates, 5 fields each), 696 for CcnA2-HA (3 biological replicates, 5 fields each), 569 for CcnA2-HA+Emi1 (3 biological replicates, 5 fields each). P-values calculated using Fisher's Exact Tests are displayed on top of the graph. Boxplots show the median (horizontal line), the interquartile range (IQR; represented by the height of the box, spanning from the 25th to the 75th percentile), and the whiskers extend from the box to the smallest and largest values within 1.5 times the IQR from the lower and upper quartiles, respectively.

**A****DNA replication (24hpi)****D****B****Pseudo-mitosis entry (96hpi)**

% of differentiating cells

**C****DNA replication (96hpi)****Pseudo-mitosis entry (24hpi)**

**Figure S8: Canonical Cyclin A2 expression in differentiating MCCs leads to abnormal mitosis figures, related to Figure 5.**

(A) Representative images of cells infected by Emi1 (96hpi), immunostained for markers of mitosis entry (top: nucleoporin, middle: actin, bottom:  $\alpha$  tubulin). Centriole staining by FOP is used to identify progenitors and differentiating deuterosomal cells. H3S10P staining is used to mark condensed chromosomes and identify mitosis or pseudo-mitosis phases. Scale bar = 10 um.

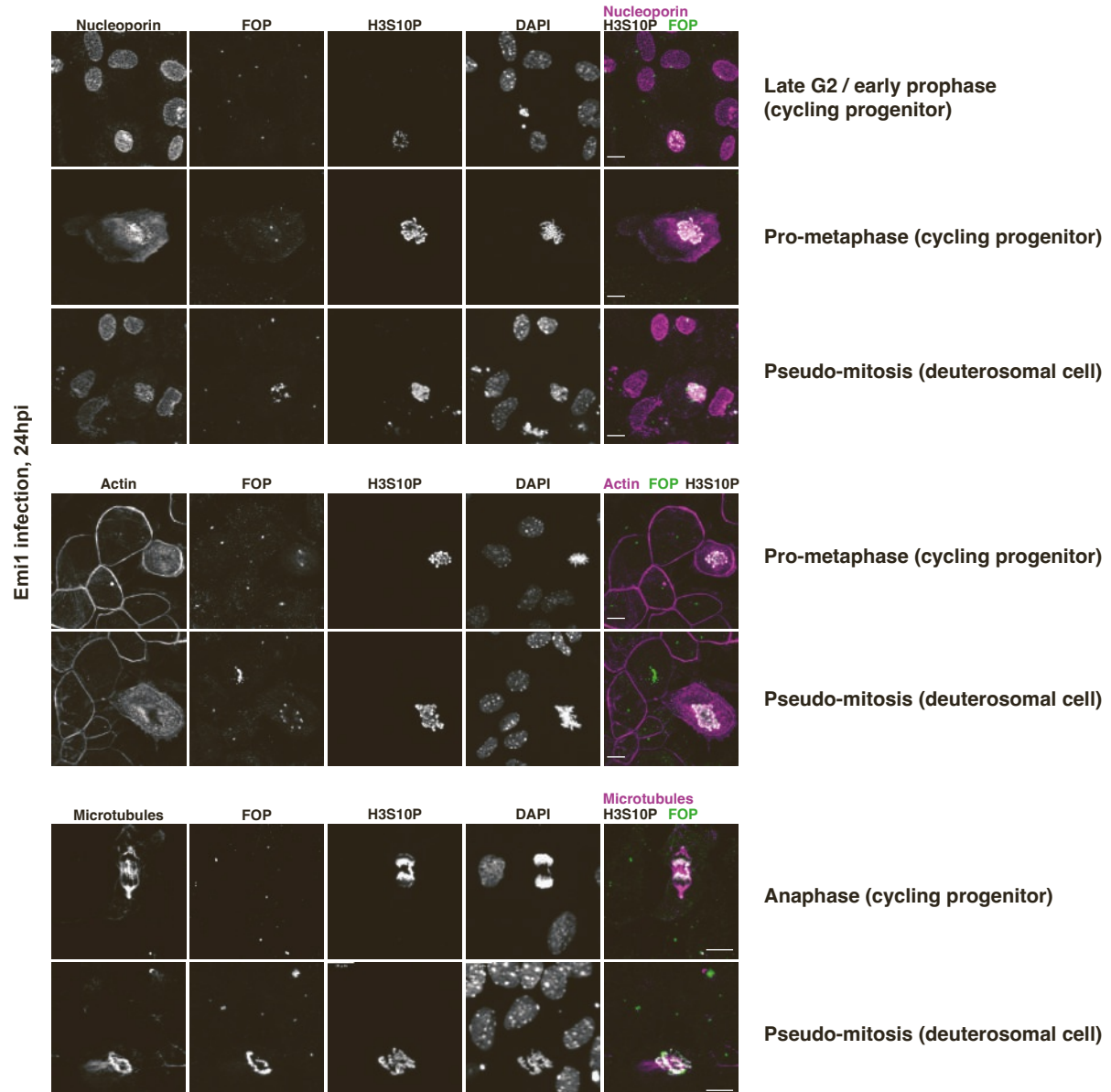


**Figure S9: Partial DNA replication can be restored in deuterosomal cells, related to Figure 6.**

- (A) Representative images of *Emi1*-infected deuterosomal cells after EdU incorporation (photos 96hpi) Chromocenters have been manually delineated with dashed lines. Note that EdU+ replicative foci are always located immediately at the periphery of chromocenters.
- (B) UMAP projection of cells undergoing MCC differentiation. Color scale represents the expression of individual factors involved in centromeric DNA replication and translesion synthesis pathway.

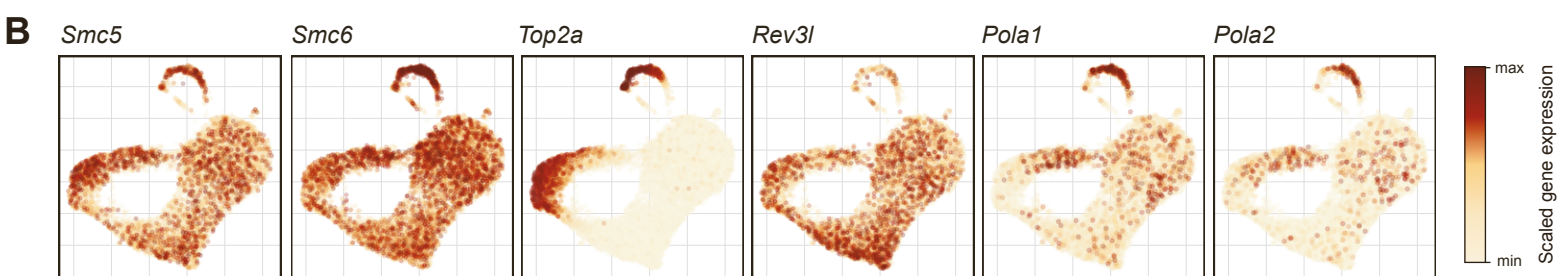
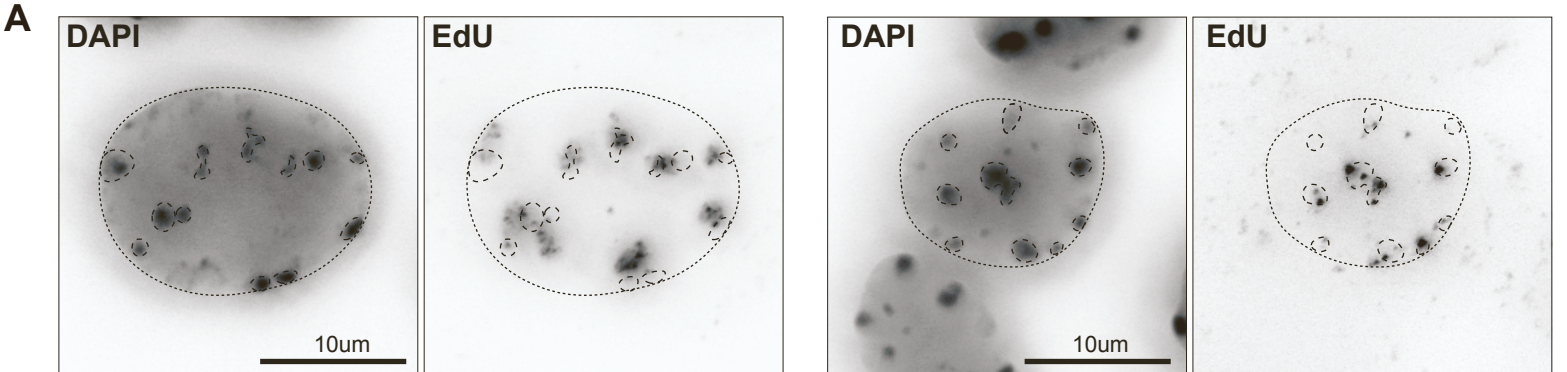
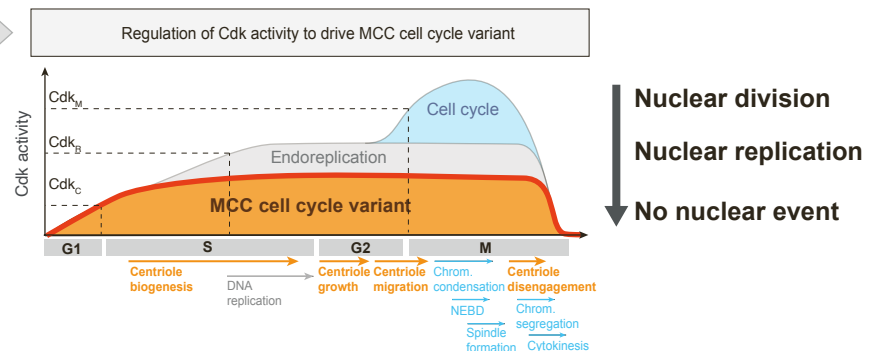
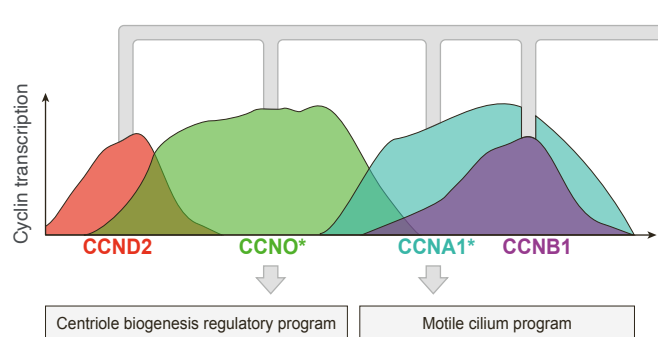


**Figure S10: Proposed model for a combined qualitative and quantitative control of CDK activity in the MCC cell cycle variant, related to Figure 6.**

Sequential waves of cyclin expression during the MCC cell cycle variant are represented (left). The temporal expression of *Ccno* and *Ccna1* is synchronized with specific transcriptional programs. The overall level of cyclins expressed in the MCC cell cycle variant also contributes to the fine-tuning of CDK activity. We propose the existence of a new  $CDK_C$  threshold, controlling the MCC cell cycle variant. We propose that in differentiating MCCs, the overall CDK activity reaches this threshold, triggering centriole biogenesis, as well as other potential cell cycle-like cytoplasmic reorganization processes. In this model, the overall CDK activity however never reaches the replication threshold ( $CDK_R$ , described in endoreplicating cells), and thus never triggers DNA replication. The  $CDK_M$  threshold, described to be above the  $CDK_R$  threshold, is therefore never attained.  $CDK_R$  and  $CDK_M$  thresholds can however be attained in MCC under CDK disinhibition.



## Supplemental references list

- [S1] O'Connor, S.A., Feldman, H.M., Arora, S., Hoellerbauer, P., Toledo, C.M., Corrin, P., Carter, L., Kufeld, M., Bolouri, H., Basom, R., et al. (2021). Neural G0: a quiescent-like state found in neuroepithelial-derived cells and glioma. *Mol. Syst. Biol.* *17*, e9522. <https://doi.org/10.15252/msb.20209522>.
- [S2] La Manno, G., Siletti, K., Furlan, A., Gyllborg, D., Vinsland, E., Mossi Albiach, A., Mattsson Langseth, C., Khven, I., Lederer, A.R., Dratva, L.M., et al. (2021). Molecular architecture of the developing mouse brain. *Nature* *596*, 92–96. <https://doi.org/10.1038/s41586-021-03775-x>.
- [S3] Ruiz García, S., Deprez, M., Lebrigand, K., Cavard, A., Paquet, A., Arguel, M.-J., Magnone, V., Truchi, M., Caballero, I., Leroy, S., et al. (2019). Novel dynamics of human mucociliary differentiation revealed by single-cell RNA sequencing of nasal epithelial cultures. *Development* *146*. <https://doi.org/10.1242/dev.177428>.
- [S4] Sikkema, L., Ramírez-Suástequi, C., Strobl, D.C., Gillett, T.E., Zappia, L., Madissoon, E., Markov, N.S., Zaragozi, L.-E., Ji, Y., Ansari, M., et al. (2023). An integrated cell atlas of the lung in health and disease. *Nat. Med.* *29*, 1563–1577. <https://doi.org/10.1038/s41591-023-02327-2>.
- [S5] Guo, J., Grow, E.J., Mlcochova, H., Maher, G.J., Lindskog, C., Nie, X., Guo, Y., Takei, Y., Yun, J., Cai, L., et al. (2018). The adult human testis transcriptional cell atlas. *Cell Res.* *28*, 1141–1157. <https://doi.org/10.1038/s41422-018-0099-2>.